IOP Publishing | Astro Ltd Laser Physics

Laser Phys. **27** (2017) 085002 (8pp) https://doi.org/10.1088/1555-6611/aa7adc

Stretching of picosecond laser pulses with uniform reflecting volume Bragg gratings

Sergiy Mokhov[1], Alexander Spiro[2], Vadim Smirnov[3], Sergiy Kaim[1], Boris Zeldovich[1] and Leonid Glebov[1]

[1] CREOL—the College of Optics and Photonics, University of Central Florida, Orlando, FL 32816, United States of America
[2] Passat, Inc., 1124 Kingsbury Rd., Owings Mills, MD 21117, United States of America
[3] OptiGrate Corp., 562 South Econ Cir., Oviedo, FL 32765, United States America

E-mail: lbglebov@creol.ucf.edu

Received 21 April 2017
Accepted for publication 19 June 2017
Published 24 July 2017

Abstract

This study shows that a uniform reflecting volume Bragg grating (VBG) can be used as a compact monolithic stretcher of high-power picosecond laser pulses, which is important for cases in which chirped Bragg gratings with the required chirp rate are difficult to fabricate. When an incident short pulse propagates along a grating and experiences local Bragg diffraction, a chirp-free reflected stretched pulse with an almost rectangular shape is generated. The increase in the duration of the reflected pulse is approximately equal to twice the propagation time along the grating. We derive an analytic expression for the diffraction efficiency, which incorporates the incident pulse duration, grating thickness, and amplitude of the refractive index modulation, enabling selection of the optimum grating for pulse stretching. Theoretical models of the extended pulse profiles are found to be in good agreement with experimental autocorrelation measurements. We also propose a simple and reliable method to control the temporal parameters of high-power picosecond pulses using the same laser source and a VBG of variable thickness, which can simplify experiments requiring different pulse durations significantly.

Keywords: pulse stretching, picosecond pulse, volume Bragg grating

(Some figures may appear in colour only in the online journal)

1. Introduction

High-power short laser pulses are widely used in various applications involving strong laser-matter interactions, such as laser material processing [1, 2], tissue ablation in medicine [3, 4], and ion acceleration from solids in experimental high-energy physics [5, 6]. The mechanisms and the results of these interactions depend on the power density, the duration of the laser energy deposition, and the material properties. These behaviors have stimulated studies of processes occurring in different materials under high-power excitation with laser pulses of variable duration. In particular, the appropriate choice of pulse duration within the femto- and picosecond ranges helps to optimize ablation regimes in different materials, allowing the required quality, rate, and cost of processing to be achieved [7–11].

Two approaches have typically been employed to vary laser pulse duration, i.e. multi-laser and single-laser techniques. The multi-laser approach involves the use of different lasers with different pulse durations [1, 2, 7], and the range and specific value of the pulse width are limited by the number of available lasers. The obvious disadvantage of this method is the need for both realignment of the optical system after laser replacement and adjustment of the focusing optics for different beam configurations from different lasers. In contrast, the single-laser approach, which has been employed in [8–11], is based on a standard technique utilizing compression of chirped femtosecond pulses by pairs of surface diffraction gratings [12]. The pulse width is varied by altering the grating distance and can be expanded up to hundreds of picoseconds. However, this technique typically requires expensive femtosecond laser equipment and precise control of the grating

alignment after each distance change. In addition, application of this technique with high-power pulses is limited by the low damage threshold of the surface gratings and by difficulties regarding the stretching of pulses with initial durations of a few picoseconds or longer. The development of laser systems with variable pulse duration in picosecond range continues mostly with the utilization of surface diffraction gratings [13, 14]. A simple method to control the duration of short laser pulses can be also implemented based on apparatus containing a dispersive element and focusing optics [15]. However, in that case, the controllable pulse width exists in the near diffraction zone in the focal plane only. Depending on whether or not a sample is placed before or after the focal plane, the different regions on the sample are pumped at different times.

A relatively new type of optical element, a volume Bragg grating (VBG) in photo-thermo-refractive (PTR) glass, has been successfully employed for the spectral and spatial control of laser radiation, including in high-power applications [16]. Volume chirped Bragg gratings (CBGs), with grating periods that gradually vary along the beam propagation direction, have been used as high-power pulse controls (for stretching and compressing) in femtosecond pulse amplification schemes [17, 18]. These optical elements have an acceptable level of optical loss, and the primary advantage of their use in pulse operations is their mechanical robustness and compactness [19]. However, the current developmental stage of the manufacturing technology used to produce CBGs in PTR glass does not facilitate the fabrication of CBGs for the stretching of pulses with initial durations of a few picoseconds or longer; this problem arises because the required low longitudinal chirp rate is difficult to achieve for the parameters of a typical holographic recording setup. This fact has stimulated the present authors to develop an alternative approach to stretching high-power picosecond laser pulses based on uniform VBGs. Besides their compactness and robustness, the obvious advantages of VBGs include their high optical damage threshold and their conservation, or even improvement, of the initial beam quality. In addition, system realignment is not required when the pulse duration is changed.

In this paper, we discuss theoretical modeling and present experimental results showing the control of pulse temporal parameters using uniform reflective VBGs. This control may be beneficial for pulse stretching in the picosecond region, for which CBGs with the required chirp rates are unavailable. In the proposed approach, the thickness of the uniform reflective VBG should be larger than the spatial length of the incident pulse, so that the duration of the stretched reflected pulse is defined by the grating thickness. In this case, the spectral bandwidth of the grating should be less than the spectral width of the incident pulse. Therefore, unlike a CBG, a uniform VBG reflects a portion of the incident pulse energy only, which is proportional to the selected part of the spectrum. It is possible to compensate for the reduction in the energy of the diffracted stretched pulses that results from the spectral narrowing via the commonly used method of long-pulse amplification. This approach has been employed in the development of custom lasers, through the incorporation of a uniform VBG stretcher in the multipass amplifier of a picosecond laser Compiler (Passat, Inc) for generation of stretched pulses with no reduction in the output pulse energy and using the same laser head dimensions.

The mechanism of short pulse reflection from Bragg gratings with narrow spectral selectivity has been theoretically studied via numerical modeling in several works [20–22]. Below, we present a theoretical analysis considering the actual parameters of the uniform VBG and the laser pulse used in our experiment, in order to demonstrate the robustness of such a technique and, also, to prove the adequacy of our modeling procedures. One of the particular procedures performed in section 3 is the quantitative rectification of the local amplitude of the refractive index modulation (RIM), based on the experimental reflection spectrum of an actual VBG with longitudinal non-uniformities.

In the final section, we discuss the general properties of short pulse reflection by a uniform Bragg grating and provide simple analytical formulas for estimating the pulse duration and reflection efficiency. Finally, we propose a reflective VBG design having uniform modulation, in which the thickness varies along the transverse coordinate. This simple and robust monolithic device would enable researchers to change the lengths of reflected pulses. Thus, it is a potentially useful tool for finding optimal laser processing regimes in various applications.

2. Coupled wave propagation equations

Pulse propagation inside a VBG is considered here, using a 1D coordinate framework. We assume that the laser beams have quite a wide aperture; thus, they do not demonstrate significant angular divergence across the grating aperture, and they propagate along a grating vector (perpendicularly to the Bragg modulation fringe planes, which are parallel to the VBG plate surfaces).

Let us begin with the wave equation for the electric field amplitude $E(z, t)$ inside a medium with refractive index $n(z)$, which is periodically modulated by the middle-to-top amplitude n_1 of the RIM at the Bragg wavelength λ_0 in vacuum. Then,

$$\begin{aligned} &\left(\partial^2/\partial z^2 - \tfrac{n(z)^2}{c^2}\partial^2/\partial t^2\right) E(z,t) = 0, \\ &n(z) = n_0 + n_1\cos(Qz + \gamma), \quad n_1 \ll n_0, \\ &Q = 2k_0, \quad k_0 = 2\pi n_0/\lambda_0 = n_0\omega_0/c. \end{aligned} \tag{1}$$

Here n_0 is the background refractive index and c is the speed of light. With skew incidence at the VBG, the resonant wavelength shifts to $\lambda_{\text{res}} = \lambda_0\cos\theta_{\text{in}}$, where θ_{in} is the propagation angle relative to the z-direction inside the VBG. The phase term γ is constant for a uniformly modulated Bragg grating and can typically be omitted. However, if the grating has non-uniformities, longitudinal deviations of the local Bragg resonant condition can then be represented as a slowly varying functional dependence $\gamma(z)$.

The $E(z, t)$ inside the Bragg grating can be conveniently represented as the sum of two counter-propagating waves $\exp(\pm ik_0 z - i\omega_0 t)$, with slowly varying complex amplitude envelopes $A(z, t)$ and $B(z, t)$, such that

$$E(z,t) = [A(z,t)\mathrm{e}^{\mathrm{i}k_0 z} + B(z,t)\mathrm{e}^{-\mathrm{i}k_0 z}]\mathrm{e}^{-\mathrm{i}\omega_0 t} + \text{c.c.} \quad (2)$$

By substituting equation (2) into the wave equation (1) and performing simplifications (including elimination of residual terms with second-order derivatives), we obtain the following system of coupled equations:

$$\begin{cases} \left(\frac{\partial}{\partial z} + \frac{n_0}{c}\frac{\partial}{\partial t}\right)A = \mathrm{i}\kappa B\mathrm{e}^{\mathrm{i}\gamma}, \\ \left(\frac{\partial}{\partial z} - \frac{n_0}{c}\frac{\partial}{\partial t}\right)B = -\mathrm{i}\kappa A\mathrm{e}^{-\mathrm{i}\gamma}, \end{cases} \quad \kappa = \pi n_1/\lambda_0, \quad (3)$$

where κ is a coupling parameter proportional to n_1 that in general can depend on the z coordinate.

For a particular temporal envelope $A(z = 0, t)$ of an incident pulse, the expressions given in equation (3) can be solved explicitly in the time domain. On the other hand, calculations can be performed in the frequency domain by decomposing slowly varying envelope profiles into their spectral components

$$a(z,\Omega) = \int A(z,t)\mathrm{e}^{\mathrm{i}\Omega t}\mathrm{d}t, \quad A(z,t) = \tfrac{1}{2\pi}\int a(z,\Omega)\mathrm{e}^{-\mathrm{i}\Omega t}\mathrm{d}\Omega. \quad (4)$$

The Fourier transforms for envelope B are similar. Substituting these transforms into equation (3) yields a system of ordinary differential equations

$$\frac{\mathrm{d}}{\mathrm{d}z}\begin{pmatrix} a \\ b \end{pmatrix} = \begin{pmatrix} \mathrm{i}\frac{n_0}{c}\Omega & \mathrm{i}\kappa\mathrm{e}^{\mathrm{i}\gamma} \\ -\mathrm{i}\kappa\mathrm{e}^{-\mathrm{i}\gamma} & -\mathrm{i}\frac{n_0}{c}\Omega \end{pmatrix}\begin{pmatrix} a \\ b \end{pmatrix}. \quad (5)$$

In the case of an arbitrary Bragg grating, the parameters κ and γ depend on the z coordinate, as mentioned above. These parameters are constant for a uniform Bragg grating, which allows integration of equation (5) and yields analytical expressions for the reflection r and transmission u coefficients, which are discussed below.

3. Spectral properties of uniform VBG

The spectral properties of reflective Bragg gratings were first efficiently described in terms of 1D coupled wave theory by Kogelnik [23]; this work was then expanded upon by many others. Here, we review the primary theoretical results using the notation employed in this study; these findings will later be used in the analysis of our experimental results.

A well-known analytical solution of the system given in equation (5) has been presented in the following transfer matrix form [24]:

$$\begin{pmatrix} a(l) \\ b(l) \end{pmatrix} = \begin{pmatrix} \alpha^* & \beta^* \\ \beta & \alpha \end{pmatrix}\begin{pmatrix} a(0) \\ b(0) \end{pmatrix}, \quad \alpha = \cosh G - \mathrm{i}\tfrac{\Phi}{G}\sinh G, \quad \beta = -\mathrm{i}\tfrac{S}{G}\mathrm{e}^{-\mathrm{i}\gamma}\sinh G,$$
$$|\alpha|^2 - |\beta|^2 = 1, \quad G = \sqrt{S^2 - \Phi^2}, \quad S = \kappa l = \pi n_1 l/\lambda_0,$$
$$\Phi = n_0 c^{-1}\Omega l \approx -2\pi n_0 l\lambda_0^{-2}\Lambda, \quad \Lambda = \lambda - \lambda_0. \quad (6)$$

Here, the dimensionless parameter S is the so-called 'strength of reflection' and Φ is the dimensionless phase detuning, which is proportional to the frequency shift Ω out of the Bragg resonance or to the wavelength shift Λ. Both S and Φ are proportional to the grating length l.

The matrix solution given in equation (6) defines the amplitude reflection coefficient r according to the boundary condition $b(l) = 0$, such that

$$r = \tfrac{b(0)}{a(0)} = -\tfrac{\beta}{\alpha}, \quad R(\Phi) = |r|^2 = \tfrac{\sinh^2 G}{\cosh^2 G - \Phi^2/S^2}, \quad R(0) = \tanh^2 S, \quad u = \tfrac{a(l)}{a(0)} = \tfrac{1}{\alpha}, \quad T = |u|^2 = 1 - R. \quad (7)$$

To derive the amplitude transmission coefficient denoted by letter u, we used the fact that the matrix determinant is unity, which follows from equation (6). The intensity reflectivity and transmissivity are R and T, respectively, and the notation used to express the mathematical values in equation (7) are defined in equation (6).

To experimentally demonstrate pulse stretching and to verify the presented theory, we employed a uniform VBG with thickness $l = 7.77$ mm, which was capable of reflecting at a laser wavelength of 1064 nm at an angle of incidence of approximately 3° in air. At this wavelength, the refractive index of PTR glass is $n_0 = 1.485$. The VBG reflection spectrum, which was experimentally measured using a tunable laser, exhibited a resonant peak at $\lambda_0 = 1064.9$ nm, with a full width at half maximum (FWHM) bandwidth equal to $\Lambda_{\mathrm{VBG,expt}} = 61$ pm and maximum reflectivity $R_{0,\mathrm{expt}} = 30\%$. According to equation (7), this corresponds to an experimentally measured strength of reflection $S_{\mathrm{expt}} = 0.61$. This S_{expt} value allowed the RIM amplitude to be estimated from equation (6) as $n_{1,\mathrm{expt}} = 27$ ppm. By taking this number and performing calculations for the reflection spectrum $R(\Phi(\Lambda))$ of the uniform VBG, using equations (6) and (7), we obtained a theoretical value of $\Lambda_{\mathrm{VBG,theor}} = 49$ pm for the FWHM bandwidth, which is noticeably smaller than the experimental result.

This discrepancy between the experimental and theoretical values of the bandwidths can be explained by acknowledging the presence of fluctuations in both the holographic interference fringe pattern and refractive index of glass along the relatively large l of the manufactured VBG. As mentioned above, such non-uniformities can be represented as unknown phase variation $\gamma(z)$ in the coupling factors in equation (5), and this variable deviation from the uniform Bragg coupling causes broadening of the resonant peak width and lowering of the resonant peak maximum. To incorporate the effects of non-uniformities and for a more accurate estimation of n_1, we employed the fact that the integral value of $R(\Phi(\Lambda))$ over a wavelength region is conserved for weakly reflective distributed feedback systems.

Let us discuss this statement in more detail. With Born approximation of small total wave coupling, we assume that an incident pulse propagating along the grating essentially conserves its energy; thus, we can neglect the term containing $b(z)$ in the first expression of equation (5) and regard $a(z)$ as the phase oscillating function. With this assumption, we can represent the amplitude reflection coefficient r_{Born} via integration of the second coupled equation in equation (5) by itself, with a standard boundary condition $b(l) = 0$. Thus,

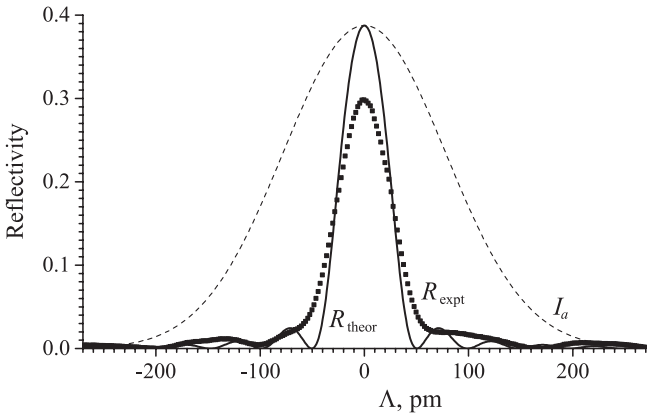

Figure 1. Experimental reflection spectrum R_{expt} of fabricated VBG (dotted line) and theoretical reflection spectrum R_{theor} of corresponding uniform VBG (solid line) with adjusted spectrum I_a of incident short 9.3 ps Gaussian pulse (dashed line).

$$a_{Born} = a(0)e^{i\Phi z/l}, \quad \frac{d}{dz}(b_{Born}e^{i\Phi z/l}) = -i\kappa e^{2i\Phi z/l - i\gamma(z)}a(0),$$
$$b(l) = 0 \quad \rightarrow \quad r_{Born}(\Phi) = \frac{b(0)}{a(0)} = i\kappa \int_0^l e^{2i\Phi z/l - i\gamma(z)}dz. \tag{8}$$

Subsequently, the dimensionless integral of the spectral reflectivity R_{Born} can be calculated with intermediate simplification through recognition of the delta function in the integral representation, such that

$$R_{Born} = |r_{Born}|^2, \quad \int e^{2i\Phi(z_1-z_2)/l}\,d\Phi = \pi l\delta(z_1 - z_2) = F_\delta,$$
$$\int R_{Born}d\Phi = \kappa^2 \int_0^l dz_1 \int_0^l dz_2 e^{i(\gamma(z_2)-\gamma(z_1))}F_\delta = \pi S^2. \tag{9}$$

Here, S is the strength of reflection previously introduced in equation (6).

We obtained that, in the case of a weak reflective Bragg grating for which Born approximation is valid, the integral of the reflection spectrum does not depend on the $\gamma(z)$ caused by unpredictable non-uniformities. This fact can be used to estimate n_1 that is more accurate than the $n_{1,expt}$ value calculated simply from the experimentally measured $R_{0,expt}$ of the actual VBG, which was residually distorted following the manufacturing process.

Figure 1 shows the experimental reflection spectrum R_{expt} of an actual VBG and the approximated theoretical spectrum R_{theor} of the uniform VBG obtained from equation (7), for a theoretical RIM amplitude $n_{1,theor} = 31.8$ ppm and corresponding theoretical strength of reflection $S_{theor} = 0.73$ according to equation (6). These adjusted parameters yield the same integral value for both spectra over the 400 pm range. We employed this limitation in the integration in order to prevent the measurement errors from having a significant influence at under large wavelength detuning. The spectrum I_a of a pulse with a Gaussian temporal profile and an FWHM time duration of 9.3 ps is also presented, in order to demonstrate the relationship between the VBG bandwidth and the pulse bandwidth used in our experiment. We will discuss the properties of pulse reflection by VBG in the next section.

The theoretical spectrum R_{theor} of a purely uniform VBG with the same thickness l and the same fit total integral of spectral reflectivity as that given in equation (9) is characterized by a higher resonant reflectivity $R_{0,theor} = 38.8\%$ and a narrower bandwidth $\Lambda_{VBG,theor} = 51.7$ pm. The suggestion of the same integral area for the R_{expt} and R_{theor} of a VBG is based on the Born approximation discussed above, and its validity is supported by the fact that the value of the numerical integral for R_{theor} is only 15% less than the simple approximated value πS^2 given in equation (9). For higher S, the proposed procedure for estimation of $n_{1,theor}$ is less accurate.

4. Temporal profiles of pulses produced by VBG

In this section, we analyze the shapes of reflected and transmitted pulses occurring after interaction of an incident short pulse with a uniform VBG. In the experiment, we used laser pulses at 1064 nm with an FWHM duration of $T_p = 9.3$ ps. Note that the experimental results of the autocorrelation measurements are discussed in section 5. The temporal amplitude profile of the incident pulse was assumed to Gaussian, $A(z = 0, t)$, and the corresponding FWHM pulse bandwidth Ω_p in the frequency domain and the FWHM spectral bandwidth Λ_p were calculated according to equation (4). Hence, the well-known relations for transform-limited Gaussian pulse profiles were employed:

$$A(0,t) = e^{-2\ln(2)t^2/T_p^2}, \quad a(0,\Omega) = \int A(0,t)e^{i\Omega t}dt =$$
$$= \frac{2\sqrt{2\pi\ln(2)}}{\Omega_p}e^{-2\ln(2)\Omega^2/\Omega_p^2} \quad \propto \quad a(\Lambda) = e^{-2\ln(2)\Lambda^2/\Lambda_p^2},$$
$$\Omega_p = 4\ln(2)/T_p, \quad \Lambda_p = \Omega_p\lambda_0^2/(2\pi c). \tag{10}$$

For the given values of T_p and λ_0, we obtained $\Lambda_p = 179$ pm for the incident pulse. The corresponding Gaussian spectrum $I_a(\Lambda) = a^2(\Lambda)$ at $z = 0$, which is adjusted to the theoretical spectrum of VBG, is presented in figure 1.

The energy efficiency η of the reflected pulse generation can be calculated simply using the VBG reflection spectrum $R(\Lambda)$ obtained from equations (6) and (7), along with the arbitrary normalized incident pulse spectrum $I_a(\Lambda)$

$$\eta = \int R(\Lambda)I_a(\Lambda)d\Lambda \Big/ \int I_a(\Lambda)d\Lambda, \quad I_a(\Lambda) = a^2(\Lambda). \tag{11}$$

For the numerical values presented above, the theoretical energy efficiency of the pulse reflection was equal to $\eta_{theor} = 10.6\%$. However, the value η measured during the experiment could be slightly lower for various reasons, one of which is that the experimental $R(\Lambda)$ of the actual VBG is slightly wider and lower than R_{theor} (figure 1). As a result, the integration of a more extended VBG reflection spectrum with a Gaussian pulse spectrum yields a smaller value in the numerator of equation (11).

The temporal amplitude profile $B(z = 0,t)$ of a reflected pulse is calculated via the inverse Fourier transformation of its amplitude profile $b(\Omega)$, using equation (4), and this amplitude profile is determined in the frequency domain by the amplitude reflection coefficient r of the VBG, equation (7), where

$$b(0,\Omega) = r(\Phi(\Omega))a(0,\Omega), \quad B(0,t) = \frac{1}{2\pi}\int b(0,\Omega)e^{-i\Omega t}d\Omega. \tag{12}$$

In a similar manner, the temporal profile of a pulse transmitted through the VBG and measured at the opposite side of the grating $A(z = l, t)$ can be calculated using the transmission coefficient u from equation (7)

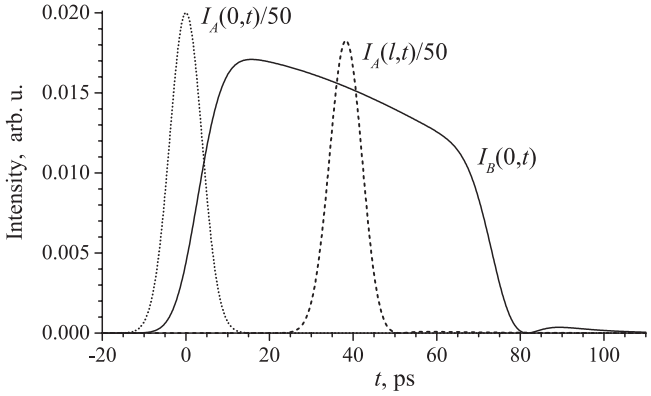

Figure 2. Calculated temporal intensity profiles: I_A of an incident pulse at $z = 0$ (dotted line); I_A of transmitted pulse at $z = l$ (dashed line); and I_B of a reflected pulse (solid line). Note that the magnitudes of the incident and transmitted profiles are reduced 50 fold.

$$a(l,\Omega) = u(\Phi(\Omega))a(0,\Omega), \quad A(l,t) = \tfrac{1}{2\pi}\int a(l,\Omega)\mathrm{e}^{-\mathrm{i}\Omega t}\mathrm{d}\Omega. \tag{13}$$

The corresponding temporal intensity profiles of the incident $I_A(0, t)$, reflected $I_B(0, t)$, and transmitted $I_A(l, t)$ pulses are

$$I_A(0,t) = |A(0,t)|^2, \;\; I_B(0,t) = |B(0,t)|^2, \;\; I_A(l,t) = |A(l,t)|^2. \tag{14}$$

Then, the same energy efficiency η of the reflected pulse generation given in equation (11) can also be calculated in the time domain, according to

$$\eta = \int I_B(0,t)\mathrm{d}t \Big/ \int I_A(0,t)\mathrm{d}t. \tag{15}$$

The η_{theor} value indicating the pulse reflection efficiency, 10.6% is relatively small for the parameters of our experiment, as a result, the shape of the $I_A(l,t)$ profile calculated at the opposite side of the VBG should be similar to that of the $I_A(0, t)$ profile, with an additional shift due to the time delay $T_{\mathrm{VBG}} = n_0 l/c = 38.5$ ps of the propagation inside the grating. The results of the calculations performed using equations (12)–(14), which are presented in figure 2, confirm these conclusions regarding the shape of the transmitted pulse.

The $I_A(0, t)$ profile was obtained with the maximum initial value equal to unity, using equations (10) and (14), and both the $I_A(0, t)$ and $I_A(l, t)$ profiles are presented in figure 2. A reduction factor of 50 was applied to these data in order to facilitate comparison between these profiles and that of $I_B(0, t)$.

In our experiment, we employed a VBG with a resonant reflectivity of less than 50%, because the pulse profile reflected from a significantly stronger grating would be more distorted and less transform-limited. This behavior is demonstrated via numerical simulation in the final section 6.

5. Autocorrelation measurements of pulse durations

In the previous section, we calculated the profiles of pulses produced by a uniform VBG with the theoretical parameters determined in section 3. In this section, the obtained numerical results are compared with experimental data for the pulse reflection efficiency and for pulse durations measured using an autocorrelation technique.

This experiment was performed using a compact commercial picosecond laser Compiler (Passat, Inc.), which provided 9 ps pulses at 1064 nm with a 400 Hz pulse repetition rate. This laser is based on Raman compression of nanosecond pulses at 1064 nm, followed by a frequency shift back to the fundamental wavelength and amplification in a multipass amplifier [2]. The average energy of an incident pulse on the VBG was $E_A = 485$ μJ, and the average energy of a reflected pulse was $E_B = 43$ μJ; hence, the experimental reflected efficiency given by their ratio was $\eta_{\mathrm{expt}} = E_B/E_A = 8.9\%$. Note that this value is close to the theoretical value of 10.6% specified in section 4. Autocorrelation measurements were performed using non-collinear second harmonic generation (NSHG). A 1064 nm beam was split in two, and there was a mechanically adjustable relative time delay τ between the resultant beams. Both beams were then focused and crossed at a small angle in a thin potassium titanyl phosphate (KTP) crystal of 1 mm thickness, in order to produce NSHG signals at 532 nm, which were measured for different τ. The radius of operated pulses was $w_0 = 1.9$ mm describing the transverse Gaussian profile of intensity as $\exp(-2r^2/w_0^2)$. With the laser power used, no distortions of transverse profiles of reflected pulses were detected which confirms the suitability of VBGs in PTR glass for reliable operation with different laser powers. Thus, we discuss theoretical and experimental results only within the framework of a 1D longitudinal approach in this paper.

The intensity autocorrelation functions for the $I_A(0, t)$ and $I_B(0, t)$ profiles are defined by

$$U_A(\tau) = \int I_A(t)I_A(t-\tau)\mathrm{d}t, \quad U_B(\tau) = \int I_B(t)I_B(t-\tau)\mathrm{d}t. \tag{16}$$

In these expressions, the zero z-coordinate of the pulse intensities have been omitted in order to emphasize that our primary focus is analysis of the temporal dependences of the pulse intensities.

The experimental and theoretical results of the autocorrelation procedures are presented in figure 3. The dots indicate the experimental measurements of U_A and U_B for the $I_A(0,t)$ and $I_B(0,t)$ profiles, while the dotted lines are their Gaussian fits. In addition, the solid line is the simulation autocorrelation function $U_B(\tau)$ calculated using equation (16), for the $I_B(0,t)$ obtained in the previous section and presented in figure 2.

The narrow Gaussian fit of the autocorrelation measurements for the incident pulse shown in figure 3 yields an FWHM peak width equal to 13.2 ps. This value is $\sqrt{2}$ times smaller than the FWHM pulse duration $T_{\mathrm{p}} = 9.3$ ps of $I_A(0,t)$, according to equations (10), (14), and (16):

$$I_A(t) = \mathrm{e}^{-4\ln(2)t^2/T_{\mathrm{p}}^2} \;\; \rightarrow \;\; U_A(\tau) \propto \mathrm{e}^{-2\ln(2)\tau^2/T_{\mathrm{p}}^2}. \tag{17}$$

We used this value of T_{p} for the numerical simulations described above, beginning with the calculation of the incident pulse amplitude $a(0, \Omega)$ in the frequency domain according to equation (10). Then, applying $a(0, \Omega)$ together with the amplitude reflection coefficient $r(\Omega)$ of a uniform VBG, from

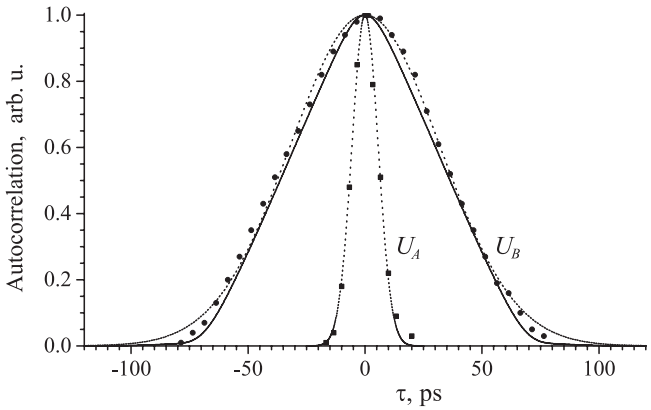

Figure 3. Normalized intensity autocorrelation functions U_A and U_B for short incident and extended reflected pulse profiles. The dots represent experimental data and the dotted lines represent corresponding Gaussian fits. The solid line is the calculated intensity autocorrelation function U_B for the reflected pulse profile I_B presented in figure 2.

equations (7) and (6), we calculated the temporal amplitude profile $B(0, t)$ of the reflected pulse using equation (12). The corresponding intensity profile $I_B(0,t)$ is shown in figure 2. Autocorrelation function $U_B(\tau)$ was calculated using equation (16) and is depicted by a solid line in figure 3. It is apparent that this simulation line is in a very good agreement with the independently measured experimental values indicated by the dots.

The $I_B(0, t)$ profile shown in figure 2 has a shape that is closer to rectangular than Gaussian. As result, the corresponding $U_B(\tau)$ depicted by the solid line in figure 3 has a triangular shape, rather than the Gaussian fit indicated by the dotted line. This result follows mathematically from equation (16) for rectangular pulse shapes. The FWHM width of the Gaussian fit of the experimental data for $U_B(\tau)$ is 75.1 ps. Thus, the corresponding temporal FWHM duration of the possible fit Gaussian pulse should be smaller by a factor of $\sqrt{2}$, according to equation (17), i.e. $T_{\mathrm{G,fit}} = 53.1$ ps. In reality, the duration of the reflected pulse can be estimated as $T_{\mathrm{R,estim}} \approx 70$ ps, from figure 2, and this value is close to twice the propagation time along the grating thickness $2T_{\mathrm{VBG}} = 77$ ps discussed in section 4. The discrepancy between $T_{\mathrm{G,fit}}$ and $T_{\mathrm{R,estim}}$ is expected, because the actual shape of the reflected pulse is rectangular rather than Gaussian.

To conclude, we would like to emphasize that the good matching of the experimental measurements for $U_B(\tau)$ with the independently calculated simulation curve in figure 3 proves the validity of the analysis of reflection of short laser pulse by uniform VBGs.

6. General discussion of pulse reflection by VBG

In the previous sections, we presented the results of our particular experiment on pulse duration stretching using a uniform reflecting VBG. With supporting numerical simulations, we demonstrated strong self-consistency in our theoretical approach to this problem. Now, let us discuss the applicability ranges of the proposed method of temporal pulse stretching.

An extended pulse is generated through local Bragg reflection of a short incident pulse propagating in the modulated glass medium of a grating specimen. By the time the incident pulse reaches the end of grating, which occurs within the period $T_{\mathrm{VBG}} = n_0 l/c$ since the moment of initial incidence, the front of the reflected pulse will have already propagated in the opposite direction for the same T_{VBG}. As a result, the front and end of the reflected pulse are spatially separated by a distance equivalent to $2l$ in the glass medium, which has refractive index n_0, and the corresponding duration of the reflected pulse $T_{\mathrm{R,estm}}$ is double the T_{VBG} of the propagation along l. Thus,

$$T_{\mathrm{R,estim}} \approx 2T_{\mathrm{VBG}}, \quad T_{\mathrm{VBG}} = n_0 l/c. \tag{18}$$

This is the basic estimation for the time duration of a pulse reflected by a uniform VBG with weak coupling, which does not significantly distort the incident pulse; hence, the reflected pulse has an approximately uniform rectangular shape.

The important practical parameter of the entire method is the diffraction energy efficiency η of the pulse reflection process. In contrast with CBGs, a uniform VBG does not transfer the entire spectral content into the reflected pulse. Instead, the spectral content is only partially transferred, and the transferred part is determined by the spectral bandwidth of the reflecting VBG. The method of passively generating spectrally narrowed pulses proposed in this study is characterized by an inherently lower diffraction η compared with CBG-based methods. A numerical calculation of η can be performed in accordance with equation (11), using the spectral content of the incident pulse and the VBG reflection spectrum. Now, we present a simple analytical expression for the estimated efficiency η_{estm}, which could be useful for the initial design of such devices. For this purpose, we will approximate the exact reflection spectrum $R(S,\Phi)$ of a uniform VBG given in equation (7), using a Gaussian fit only and with a spectral width Φ_{VBG}, such that

$$\begin{aligned} &R = S^2/\Phi^2 \sin^2\Phi + O(S^4) \approx \tanh^2 S \cdot \Phi^{-2}\sin^2\Phi \\ &\rightarrow \quad \Phi_{\mathrm{VBG}} \approx \pi, \quad R_{\mathrm{estm}} = \tanh^2 S \cdot \mathrm{e}^{-4\ln(2)\Phi^2/\pi^2}. \end{aligned} \tag{19}$$

Here, a series expansion of R over S was employed, which gives the primary detuning dependence $\Phi^{-2}\sin^2\Phi$. In addition, the normalization of the resonant reflection maximum, which is $R_0 = \tanh^2 S$, was retained. The FWHM of the main lobe Φ_{VBG} was estimated as π, which is half the detuning range between the two first zeros of $\Phi^{-2}\sin^2\Phi$. Finally, we fit the reflection spectrum of the uniform VBG using a Gaussian curve R_{estm} with this width.

The spectrum I_a of the incident Gaussian pulse given in equation (10) can be presented in terms of the detuning parameter Φ used for analysis of the VBG spectral properties in equation (6), such that

$$\begin{aligned} &\Phi = T_{\mathrm{VBG}}\Omega, \quad \xi = T_{\mathrm{VBG}}/T_{\mathrm{p}}, \quad \Omega_{\mathrm{p}}T_{\mathrm{p}} = 4\ln(2), \\ &I_a(\Phi) = a^2(\Phi) \propto \mathrm{e}^{-4\ln(2)\Omega^2/\Omega_{\mathrm{p}}^2} = \mathrm{e}^{-\Phi^2/(4\ln(2)\xi^2)}. \end{aligned} \tag{20}$$

Here, ξ is the ratio of the propagation time T_{VBG} along a grating thickness l over pulse duration T_{p}. With the simplified estimated VBG spectrum $R_{\mathrm{estm}}(\Phi)$ obtained from equation (19), the integration in equation (11) can be performed

easily. Hence, we obtain the following estimation of the pulse reflection efficiency:

$$\eta_{\text{estm}} = \int R_{\text{estm}}(\Phi) I_a(\Phi)\mathrm{d}\Phi / \int I_a(\Phi)\mathrm{d}\Phi$$
$$= \tanh^2 S / \sqrt{1 + (4\ln(2)\xi/\pi)^2} \approx \pi \tanh^2(S)/(4\ln(2)\xi). \quad (21)$$

As the S defined in equation (6) is proportional to both l and n_1, and as ξ is proportional to l itself, then according to equation (21), for small S, η_{estm} is linearly proportional to l and quadratically proportional to n_1. Last simplification in this equation is valid for large T_{VBG} along the grating, relative to the incident pulse duration, i.e. for $\xi > 3$ at minimum. This condition is intentional, as it allows the proposed realization of the temporal pulse extension by the uniform VBG. In our case, $\xi = 4.14$ for the $T_{\text{VBG}} = 38.5\,\text{ps}$ value given above and for $T_{\text{p}} = 9.3\,\text{ps}$. With $\tanh^2 S = R_{0,\text{theor}} = 38.8\%$ being the value of the theoretical reflection maximum, we obtain $\eta_{\text{estm}} = 10.6\%$, which coincides with the η_{theor} previously calculated using equation (11). The factor $\tanh^2 S$ is kept equal to $R_{0,\text{theor}} = R(0)$ in equation (7), in order to emphasize that this value could differ from the experimentally measured value of $R_{0,\text{expt}}$, because of the distortions in the reflection spectrum caused by the $\gamma(z)$ discussed in section 2.

The temporal amplitude profile of a particular elongated reflected pulse $B(t)$ can be calculated using equation (12), via the Fourier transform of the product of the $r(\Omega)$ given in equation (7) and the $a(\Omega)$ of equation (10). The shape of a reflected pulse and the efficiency of the reflection at the exact Bragg resonance are determined by two dimensionless parameters: S and ξ. On plots in the spectral domain similar to that shown in figure 1, S defines the shape of the theoretical reflection spectrum of a VBG with its maximum $R_0 = \tanh^2 S$, and ξ defines how wide the spectrum of the incident pulse is in comparison with the VBG bandwidth. Thus, there is scalability in the mathematical description of this problem. If we have two gratings with the same R_0 but different T_{VBG}, and if they are separately exposed to pulses with respective durations of T_{p1} and T_{p2} that are in the same proportion to the grating propagation times, $T_{\text{VBG,1}}/T_{\text{p1}} = T_{\text{VBG,2}}/T_{\text{p2}}$, so that ξ is the same in both cases, the η values will be identical and the two pulse shapes will be similar to each other. The only differences between the reflected pulse shapes are their different time durations, which are proportional to the corresponding incident pulse durations.

Let us present the actual temporal intensity profiles $I_B(t)$ for different grating reflectivities $\tanh^2 S$ and ratios ξ, see equations (6) and (20). A certain tunability of these parameters can be realized in particular grating designs, because of the presence of transverse degrees of freedom in operation with VBGs. For example, besides the standard resonant wavelength shift with angular tuning of the reflective VBG [25], the variations in the grating parameters with parallel translation of the VBGs along the transverse coordinate have been used in [26], in order to tune the resonant wavelength, and in [27], so as to tune the transmission bandwidth of the resonant VBG cavity. The simplest approach to creating a VBG producing a tunable pulse duration is to cut a VBG with varying length from a glass wafer using a recorded standard uniform

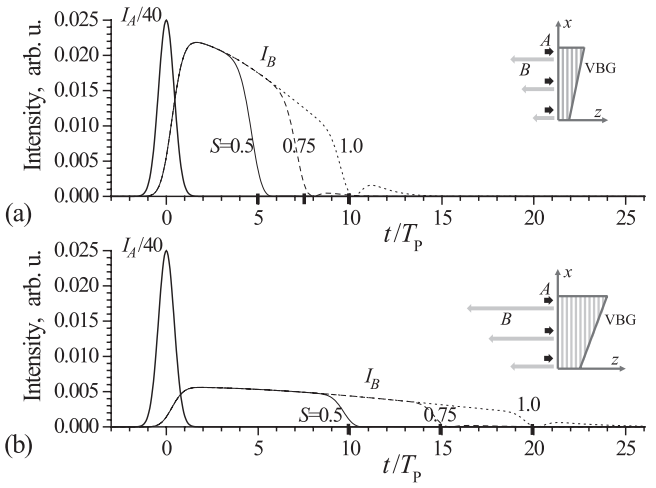

Figure 4. Modeled temporal intensity profile I_A of incident pulse reduced by a factor of 40, and temporal intensity profiles I_B of pulses reflected at points with different VBG thicknesses. These thicknesses correspond to reflection strengths $S = 0.5$, 0.75, 1 and to grating propagation times defined by the ratios: (a) $\xi = T_{\text{VBG}}/T_{\text{p}} = 2.5$, 3.75, 5; and (b) $\xi = 5$, 7.5, 10. The 2ξ values are marked on the dimensionless time scale.

modulation pattern, as shown on the right of figure 4. In this case, κ is constant and, according to equation (6), S is proportional to the grating length $l(x)$, which in turn depends on the x-position of the pulse incidence. As the incident pulse propagates orthogonally to the front surface of the VBG and to the fringes of the Bragg pattern, the quality of the reflected beam is not distorted. The longitudinal shapes of the extended pulses reflected at three different transverse positions are presented in figure 4 for two trapezoid gratings with different Bragg couplings. Note that the time coordinate on the horizontal axis is dimensionless and is measured in terms of the incident pulse width.

The calculated $I_B(t)$ exhibit durations close to the estimated values of the elongated pulse durations, $T_{\text{R,estm}} \approx 2T_{\text{VBG}}$, from equation (18). The corresponding factors $2\xi \approx T_{\text{R,estm}}/T_{\text{p}}$ are marked on the horizontal time axis. When the grating thickness and the corresponding $R_0 = \tanh^2 S$ are increased, the reflected profile becomes less uniform and a secondary peak appears. This behavior indicates that it is preferable to use a grating with relatively low reflectivity, i.e. $R_0 < 50\%$. For intermediate incidence positions with reflectivity $R_0 = \tanh^2 0.75 = 40.3\%$, the efficiency is equal $\eta_{\text{theor}} = 12.1\%$ and 6.4% for $\xi = T_{\text{VBG}}/T_{\text{p}} = 3.75$ and 7.5, respectively. These numerically calculated η_{theor} are actually approximated with good accuracy by the values η_{estm} estimated from equation (21).

The simulations presented here show that it is feasible to increase the pulse duration by a factor of 10 from 10 ps through use of a reflective uniform VBG with a total efficiency η of almost 10%. This conclusion is also supported by our experimental results. At the beginning of section 1, it was mentioned that we consider pulses that are almost normally incident on the Bragg modulation planes of the grating refractive index. In the examined process involving 1D propagation, the transverse profiles of the incident and elongated reflected pulses are preserved.

7. Conclusion

We theoretically analyzed and experimentally confirmed the stretching of high-power picosecond laser pulses with no spectral chirp via reflection from a uniform VBG. This stretching process is important for cases in which it is not possible to fabricate CBGs with the required chirp rate. Simple analytical expressions for calculating the duration of the reflected pulses and the diffraction efficiency of pulse stretching via the uniform VBG were found. The increase in the pulse duration was shown to be proportional to the grating thickness; thus, the required stretching can be achieved simply, via an appropriate choice of VBG thickness.

In our experiment, 9.3 ps pulses with Gaussian profiles were stretched to 75 ps via reflection from a uniform VBG of 7.8 mm in thickness. The reflected pulses were characterized by an almost rectangular shape, which is not typically achievable using standard methods of laser pulse generation. The experimental energy efficiency of the diffraction was approximately 9%, which is close to the calculated theoretical value of 10.6%. The latter value was calculated considering the spectral narrowing of the reflected emission. We believe that the relatively low energy efficiency of the proposed method is more than offset by a number of its advantages in comparison with a surface diffraction grating based approach. They are the chirp-free spectrum of the stretched pulse, the compactness, robustness, and preservation of the alignment and beam quality, and the tolerance to high laser power. The amplification of pulses of several tens of picoseconds or longer does not usually require special measures to avoid undesirable non-linear effects. Therefore, the low diffraction efficiency can be easily compensated using standard methods of pulse amplification. A VBG element with variable thickness facilitates gradually varying pulse duration via transverse shifting of the VBG orthogonally to the incident beam.

References

[1] Tunnermann A, Nolte S and Limpert J 2010 Femtosecond versus picosecond material processing: challenges in ultrafast precision laser micro-machining of metals at high repetition rates *Laser Tech. J.* **7** 34–8

[2] Spiro A, Lowe M and Pasmanik G 2012 Drilling rate of five metals with picosecond laser pulses at 355, 532, and 1064 nm *Appl. Phys.* A **107** 801–8

[3] Strassl M, Wieger V, Brodoceanu D, Beer F, Moritz A and Wintner E 2008 Ultra-short pulse laser ablation of biological hard tissue and biocompatibles *J. Laser Micro Nanoeng.* **3** 30–40

[4] Sajjadi A Y, Mitra K and Grace M 2011 Ablation of subsurface tumors using an ultra-short pulse laser *Opt. Laser Eng.* **49** 451–6

[5] Zhidkov A, Uesaka M, Sasaki A and Daido H 2002 Ion acceleration in a solitary wave by an intense picosecond laser pulse *Phys. Rev. Lett.* **89** 215002

[6] Daido H, Nishiuchi M and Pirozhkov A 2012 Review of laser-driven ion sources and their applications *Rep. Prog. Phys.* **75** 056401

[7] Semerok A, Sallé B, Wagner J-F and Petite G 2002 Femtosecond, picosecond, and nanosecond laser microablation: laser plasma and crater investigation *Laser Part. Beams* **20** 67–72

[8] Chichkov B N, Momma C, Nolte S, von Alvensleben F and Tunnermann A 1996 Femtosecond, picosecond and nanosecond laser ablation of solids *Appl. Phys.* A **63** 109–15

[9] Chien C Y and Gupta M C 2005 Pulse width effect in ultrafast laser processing of materials *Appl. Phys.* A **81** 1257–63

[10] Harzic R L, Breitling D, Weikert M, Sommer S, Föhl C, Valette S, Donnet C, Audouard E and Dausinger F 2005 Pulse width and energy influence in laser micromachining of metals in a range of 100 fs to 5 ps *Appl. Surf. Sci.* **249** 322–31

[11] Bian Q, Yu X, Zhao B, Chang Z and Lei S 2013 Femtosecond laser ablation of indium tin-oxide narrow grooves for thin film solar cells *Opt. Laser Technol.* **45** 395–401

[12] Treacy E B 1969 Optical pulse compression with diffraction gratings *IEEE J. Quantum Electron.* **5** 454–8

[13] Morrissey F X, Fan T Y, Miller D E and Rand D 2017 Picosecond kilohertz-class cryogenically cooled multistage Yb-doped chirped pulse amplifier *Opt. Lett.* **42** 707–10

[14] Kuptsov G V, Petrov V V, Laptev A V, Petrov V A and Pestryakov E V 2016 Simulation of picosecond pulse propagation in fibre-based radiation shaping units *Quantum Electron.* **46** 801–5

[15] Spiro A and Lowe M 2014 Method of ultrafast beam rotation for single-shot, time-resolved measurements *Opt. Lett.* **39** 5362–5

[16] Efimov O M, Glebov L B, Glebova L N, Richardson K C and Smirnov V I 1999 High-efficiency Bragg gratings in photothermorefractive glass *Appl. Opt.* **38** 619–27

[17] Glebov L, Smirnov V, Rotari E, Cohanoschi I, Glebova L, Smolski O, Lumeau J, Lantigua C and Glebov A 2014 Volume-chirped Bragg gratings: monolithic components for stretching and compression of ultrashort laser pulses *Opt. Eng.* **53** 051514

[18] Kaim S, Mokhov S, Zeldovich B Ya and Glebov L B 2014 Stretching and compressing of short laser pulses by chirped volume Bragg gratings: analytic and numerical modeling *Opt. Eng.* **53** 051509

[19] Liao K-H, Cheng M-Y, Flecher E, Smirnov V I, Glebov L B and Galvanauskas A 2007 Large-aperture chirped volume Bragg grating based fiber CPA system *Opt. Express* **15** 4876–82

[20] Yang B, Yan X, Yang Y and Zhang H 2008 Study on the instantaneous characteristics of diffracted and transmitted light of static photorefractive grating illuminated by ultrashort pulse laser *Opt. Laser Technol.* **40** 906–11

[21] Yi Y, Liu D and Liu H 2011 Instantaneous characteristics study of the diffracted and transmitted light of a static photorefractive reflection volume holographic grating read by an ultrashort pulse laser *J. Opt.* **13** 035701

[22] Yan X, Yan X, Dai Y, Yang X and Ma G 2014 Temporal diffraction characteristics of transmitted multilayer volume holographic grating illuminated by an ultrashort pulse *Optik* **125** 3231–6

[23] Kogelnik H 1969 Coupled wave theory for thick hologram gratings *Bell Syst. Tech. J.* **48** 2909–45

[24] Glebov L, Lumeau J, Mokhov S, Smirnov V and Zeldovich B 2008 Reflection of light by composite volume holograms: Fresnel corrections and Fabry-Perot spectral filtering *J. Opt. Soc. Am.* A **25** 751–64

[25] Andrusyak O, Smirnov V, Venus G and Glebov L 2009 Beam combining of lasers with high spectral density using volume Bragg gratings *Opt. Commun.* **282** 2560–3

[26] Jacobsson B, Pasiskevicius V, Laurell F, Rotari E, Smirnov V and Glebov L 2009 Tunable narrowband optical parametric oscillator using a transversely chirped Bragg grating *Opt. Lett.* **34** 449–51

[27] Mokhov S, Ott D, Divliansky I, Zeldovich B and Glebov L 2014 Moiré volume Bragg grating filter with tunable bandwidth *Opt. Express* **22** 20375–86